



CHORUS

This is the accepted manuscript made available via CHORUS. The article has been published as:

Quantum Rifling: Protecting a Qubit from Measurement Back Action

Daniel Szombati, Alejandro Gomez Friero, Clemens Müller, Tyler Jones, Markus Jerger, and Arkady Fedorov

Phys. Rev. Lett. **124**, 070401 — Published 20 February 2020

DOI: [10.1103/PhysRevLett.124.070401](https://doi.org/10.1103/PhysRevLett.124.070401)

Quantum rifling: protecting a qubit from measurement back-action

Daniel Szombati,^{1,2,*} Alejandro Gomez Friero,^{1,2} Clemens Müller,³ Tyler Jones,^{1,2} Markus Jerger,^{1,2} and Arkady Fedorov^{1,2}

¹*ARC Centre of Excellence for Engineered Quantum Systems, Queensland 4072, Australia*

²*School of Mathematics and Physics, University of Queensland, St Lucia, Queensland 4072, Australia*

³*IBM Research Zürich, 8803 Rüschlikon, Switzerland*

(Dated: January 23, 2020)

Quantum mechanics postulates that measuring the qubit’s wave function results in its collapse, with the recorded discrete outcome designating the particular eigenstate the qubit collapsed into. We show this picture breaks down when the qubit is strongly driven during measurement. More specifically, for a fast evolving qubit the measurement returns the time-averaged expectation value of the measurement operator, erasing information about the initial state of the qubit, while completely suppressing the measurement back-action. We call this regime “quantum rifling”, as the fast spinning of the Bloch vector protects it from deflection into either of its two eigenstates. We study this phenomenon with two superconducting qubits coupled to the same probe field and demonstrate that quantum rifling allows us to measure either one of the two qubits on demand while protecting the state of the other from measurement back-action. Our results allow for the implementation of selective read out multiplexing of several qubits, contributing to efficient scaling up of quantum processors for future quantum technologies.

The Stern-Gerlach experiment, originally conducted to demonstrate quantization in atomic-scale systems[1], is the prototypical example of a quantum measurement with a linear detector: an electron (or qubit) flying through a magnetic field is deflected from its straight path, with probabilities dependent on the qubit’s initial state (see Figure 1a). The measurement projects the state of the qubit onto either of its two spin eigenstates: $\pm\hbar/2$.

Driving the qubit with Rabi frequency Ω_R during the measurement leads to competition between the state evolution and the measurement projection. Such a scenario has been studied theoretically [2–4] and experimentally [5, 6] in the strong measurement regime $\Omega_R \ll \Gamma_m$, where Γ_m is the measurement rate at which information is extracted from the qubit. This regime is commonly described by the Quantum Zeno effect[7]: a strong quantum measurement freezes the qubit’s state, with occasional transitions occurring as sudden quantum jumps[8–12] with rate $\propto \Omega_R^2/\Gamma_m$.

The regime of strong driving $\Omega_R \gg \Gamma_m$, referred to as the sub-Zeno limit, has attracted attention in the context of continuous weak measurements[13]. When the probe’s bandwidth $\delta\omega$ exceeds the Rabi frequency, $\Omega_R < \delta\omega$, signatures of coherent Rabi oscillations appear in the detector signal [14–17]. It has been shown that the back-action introduced by the measurement imposes a fundamental limit on the detection of oscillations and can be used to determine the quantum efficiency of the detector[15, 18, 19], or even to test the Leggett-Garg inequality[20, 21]. The opposite limit $\Omega_R > \delta\omega$, where the Rabi frequency exceeds the bandwidth, is suitably described by the average Hamiltonian theory [22]. This regime however, has not yet been investigated in the context of continuous qubit measurement neither theoretically nor experimentally.

In this Article, we study the measurement of a continuously driven qubit in the regime where the Rabi frequency

dominates all other relevant parameters: $\Omega_R \gg \Gamma_m, \delta\omega$. First, we show that when the probe’s bandwidth is not sufficient to follow the qubit’s state, the probe signal reveals only the expectation value of the time-averaged measurement operator $\langle \sigma_z(t) \rangle = 0$, leading to the erasure of any information contained in the probe about the qubit state and thus canceling the measurement back-action on the qubit. In the language of the Stern-Gerlach experiment, the fast rotation of the spin allows the electron to fly through the measurement apparatus in a straight line without experiencing a force. Thus we call this effect quantum rifling, in analogy to the rifling of bullets, which stabilizes the trajectory of the projectile (see Figure 1b). We then investigate the driving threshold to achieve rifling by measuring the Rabi decay rate of a probed qubit for different probe field amplitudes. Finally, using tomographic reconstruction of the qubit’s state, we demonstrate read out multiplexing of two qubits coupled to the same measurement apparatus: quantum rifling is used to suppress the measurement back-action on one of the qubits on demand, while still extracting full information about the state of another qubit.

Our system consists of two superconducting transmon qubits[23] coupled dispersively to a microwave resonator[3](see Supplementary information Sec. I for details). The driven stationary microwave mode passing through the resonator acts as our measurement probe: its interaction with the qubit leads to a qubit state-dependent dispersive shift of the resonator frequency. Rifling of the qubit state is achieved by applying a resonant Rabi drive to a charge line coupled directly to the qubit. For weak Rabi driving, the resonator transmission measurement returns two peaks weighted by the corresponding populations of the ground and excited states of the qubit (see Figure 1c). When the driving strength reaches a

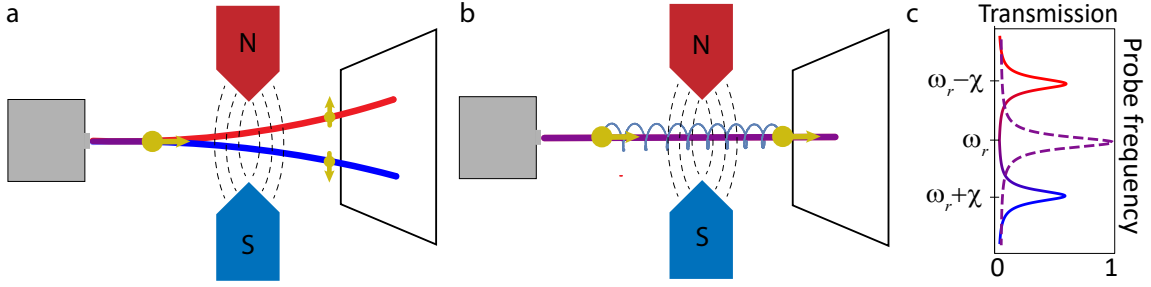


FIG. 1. **Quantum rifling in a Stern-Gerlach setup.** **a**, Measurement of a spin initially prepared in a superposition state. The magnetic field measures the spin by deflecting its flight path in a direction dependent on the measured spin orientation. **b**, Measurement during rifling; when the spin is strongly driven during measurement the magnetic field cannot discriminate between spin states and the spin's flight path is undisturbed. **c**, Detection mechanism of the qubit state in our setup; the resonator experiences a qubit state-dependent shift in its resonance frequency by $\pm\chi$ relative to its bare frequency ω_r in the rotating frame. Thus after averaging the results of experiment (a) one would observe the red and blue resonator transmission curves. During quantum rifling, when the qubit's state is driven resonantly with its transition energy, the resonator's resonance shifts to ω_r , leading to the dashed transmission curve following the averaging of the experiment presented in (b).

threshold, the transmission spectrum yields a single central peak analogous to a straight flight-path for the spin in the Stern-Gerlach apparatus.

Figure 2a shows the transmission spectroscopy of the resonator when Qubit 1 is continuously driven on resonance. Varying the qubit drive power we identify different characteristic regimes of the measurement. For low drive power the qubit remains in its ground state and only a single transmission peak is visible at $\omega_r + \chi$. As the Rabi drive becomes sufficient to excite the qubit, a second peak appears at $\omega_r - \chi$ in the cavity spectrum. The two peaks reach equal height when the qubit is saturated by the drive and the populations of the qubit in its ground and excited state becomes equal.

As Ω_R increases the two cavity peaks split, and the outer diverging peaks vanish with increasing drive. The inner peaks converge to a single peak at the average frequency ω_r , which we identify as the onset of the quantum rifling regime. When the Rabi drive becomes comparable to the transmon anharmonicity, the central cavity peak splits again as we populate higher levels, setting an upper bound on the rifling power (see Supplementary information Sec. II.).

The system can be described by the Jaynes-Cummings Hamiltonian in the dispersive regime transformed into a doubly rotating frame at both the qubit and probe drive frequencies ω_q, ω_p respectively:

$$H/\hbar = \delta\omega_r a^\dagger a + \chi a^\dagger a \sigma_z + \frac{1}{2}\epsilon_d(a^\dagger + a) + \frac{1}{2}\Omega_R \sigma_x, \quad (1)$$

where $\delta\omega_r = \omega_r - \omega_p$, a^\dagger and a are creation and annihilation operators of resonator excitation modes, $\sigma_{x/z}$ are Pauli matrices acting on the qubit, ϵ_d is the probe amplitude, and we assume resonant driving with the qubit's ground to excited state transition frequency, $\omega_q = \omega_{ge}$. Including decoherence and losses for such a system[24],

the full time-evolution is described by the master equation

$$\dot{\rho} = -\frac{i}{\hbar} [H, \rho] + \kappa \mathcal{D}[a]\rho + \gamma_\downarrow \mathcal{D}[\sigma_-]\rho + \frac{1}{2}\gamma_\varphi \mathcal{D}[\sigma_z]\rho, \quad (2)$$

where $\mathcal{D}[o]\rho = o\rho o^\dagger - \frac{1}{2}(o^\dagger o\rho + \rho o^\dagger o)$, $\kappa/(2\pi) = 0.95$ MHz is the cavity decay rate and $1/\gamma_\downarrow$, $1/\gamma_\varphi$ are the qubit relaxation and pure dephasing times, respectively.

We compute both numerically[25] and analytically the steady-state of the resonator probe amplitude $\langle a \rangle$ by solving Eq. (2) (as well as its extension to a three-level transmon) in the low photon number limit $\langle n_{\text{photon}} \rangle \approx 0$, plotting the result in Figure 2b-c. The additional splitting of the central resonance peak around $\Omega_R/(2\pi) \approx 100$ MHz is well accounted for by the multi-level model.

When truncated to the single cavity photon subspace, the diagonalization of the Hamiltonian (1) for $\epsilon_d = 0$ leads to four eigenstates in the dressed-state picture[26, 27], each a superposition of both atom and resonator states. Note that these dressed states are of quantum origin leading to entanglement between the cavity field and the qubit, as opposed to e.g. the Mollow-triplet, where the qubit is dressed classically. The unnormalized expressions are:

$$\begin{aligned} |0\pm\rangle &\sim |g, 0\rangle \pm |e, 0\rangle, \\ |1\pm\rangle &\sim \frac{2\chi \pm \sqrt{4\chi^2 + \Omega_R^2}}{\Omega_R} |g, 1\rangle + |e, 1\rangle, \end{aligned} \quad (3)$$

where $|g, e\rangle$ are the ground- and excited states of the qubit and $|n\rangle$ are resonator states with n photons. The corresponding eigenenergies in the rotating frame at $\delta\omega_r = 0$ can be found as $E_{0\pm} = \pm\frac{1}{2}\hbar\Omega_R$ and $E_{1\pm} = \pm\frac{1}{2}\hbar\sqrt{4\chi^2 + \Omega_R^2}$.

The four cavity transmission peaks correspond to the four transitions between eigenstates with differing photon parity (see Figure 2b dashed lines). In the limit of $\Omega_R \ll \kappa$, $E_{0-} \approx E_{0+}$ yielding two degenerate transitions

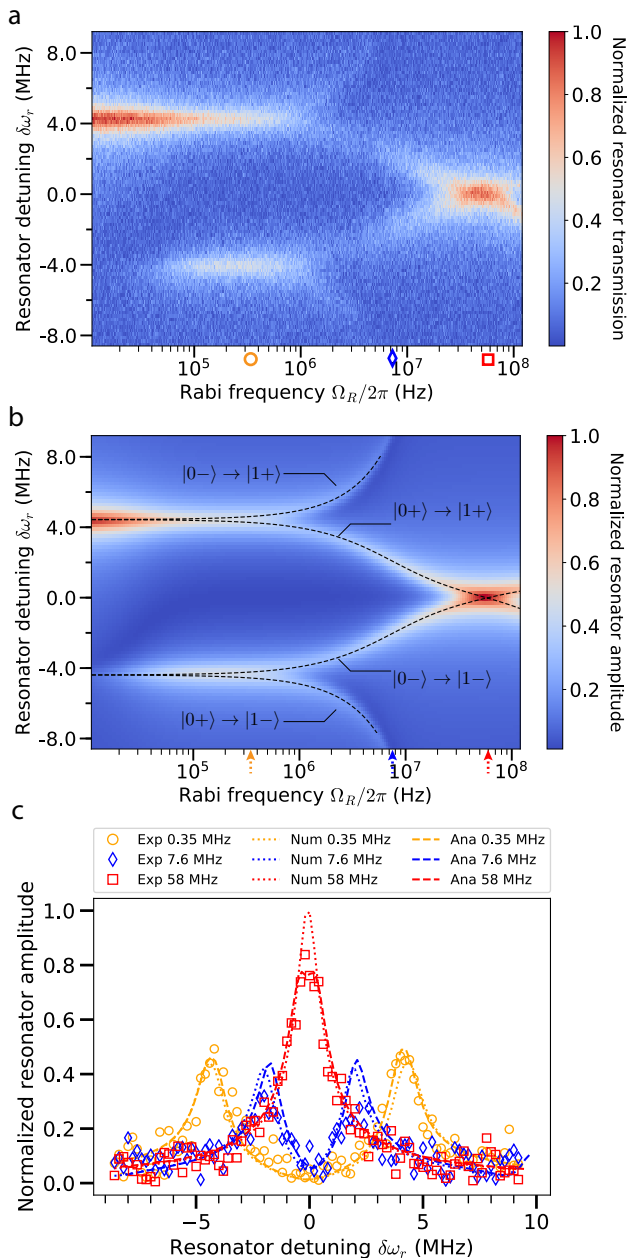


FIG. 2. **Resonator spectroscopy vs Rabi drive strength.** **a**, Continuous wave spectroscopy of the resonator transmission vs. Rabi frequency. The resonator is probed by a mean photon number of $\langle n_{\text{photon}} \rangle \approx 0.13$. The symbols below the plot show the qubit drive strength at which linecuts are shown in (c). **b**, Steady-state numerical simulation of Eq.(2) extended to the three-level transmon model for the observable $|a\rangle$ plotted as a function of $\delta\omega_r/2\pi$ and $\Omega_R/2\pi$, assuming a steady-state drive and using experimental parameters quoted in the main text. Dashed lines show the transitions in frequency between the $|0\pm\rangle$ and $|1\pm\rangle$ states. The arrows under the plot show the frequencies for the line cuts in (c). **c**, Comparison of experimental data and numerical simulations presented in (a-b), as well as the analytical solution for a two-level qubit at three values of the Rabi drive strength. All data have been normalized such that the maximum amplitude without Rabi drive is 1.

at frequencies $\omega_r \pm \chi$. The splitting of the peaks is proportional to Ω_R , which becomes visible when their splitting exceeds the linewidth $\Omega_R/2\pi > \kappa/2\pi \approx 1$ MHz. In the opposite limit of strong driving $\Omega_R \gg \chi$, thus $E_0 \approx E_1$. The matrix elements corresponding to the outer transitions at $E_{0\mp} \rightarrow E_{1\pm}$ vanish for large Ω_R , making the outer peaks disappear. The inner transitions $E_{0\pm} \rightarrow E_{1\pm}$ converge in energy, merging into the central cavity peak once their separation is too small to still resolve two peaks $|E_1 - E_0|/\hbar < \kappa$, leading to the condition for the quantum rifling regime $\Omega_R > \Omega_C = \chi^2/\kappa \approx 2\pi \times 16$ MHz. For larger cavity probe powers, the evolution of the transmission peaks remains qualitatively the same, with less pronounced side peaks and the critical drive amplitude Ω_C shifting to higher drive frequencies (see Supplementary information Sec III. for details).

We have also verified that the effect of two resonator transmission peaks merging into one can also be induced by fast incoherent qubit dynamics (see Supplementary information Sec. IV.). As for a qubit interacting with a heat bath at different temperatures such that $\langle \sigma_z \rangle \neq 0$ in the steady state, simulations show that the position in frequency of the central peak shifts proportionally to the asymmetry in population between the ground and excited state (see Supplementary information Sec. II. B1).

We examine the back-action of the detector on the qubit by measuring the relaxation rate of Rabi oscillations with and without a simultaneous resonator tone. The qubit relaxes due to measurement back-action and through intrinsic losses to the environment. For low Rabi frequencies, the back-action dominates this relaxation. However, with increasing Rabi frequency the detector's ability to distinguish between the qubit eigenstates diminishes thus reducing the measurement back-action, reaching zero in the single peak regime. The results are presented in Figure 3, varying the Rabi frequency for each specific probe power.

For a Rabi drive $\Omega_R \ll \Omega_C$, the Rabi coherence time $T_R = \Gamma_R^{-1}$ is degraded by the measurement: the probe extracts information from the qubit leading to its dephasing. For strong Rabi drive $\Omega_R \gg \Omega_C$, the qubit coherence times are comparable to the standard Rabi decay time measured without applying a simultaneous cavity pulse. Driving the cavity with more photons leads to a stronger suppression of the coherence time for small Rabi frequencies, consistent with the measurement rate being proportional to the cavity's photon number population. The threshold Rabi drive frequency Ω_C at which T_R converges to the standard Rabi coherence time of the qubit is, however, independent of the cavity tone strength for low photon population ($\langle n_{\text{photon}} \rangle \ll 1$). This is in agreement with the observed threshold drive required for the emergence of a single cavity peak in continuous wave spectroscopy (see Figure 2 and Supplementary information Sec. III.).

We also numerically simulate such rifled Rabi oscilla-

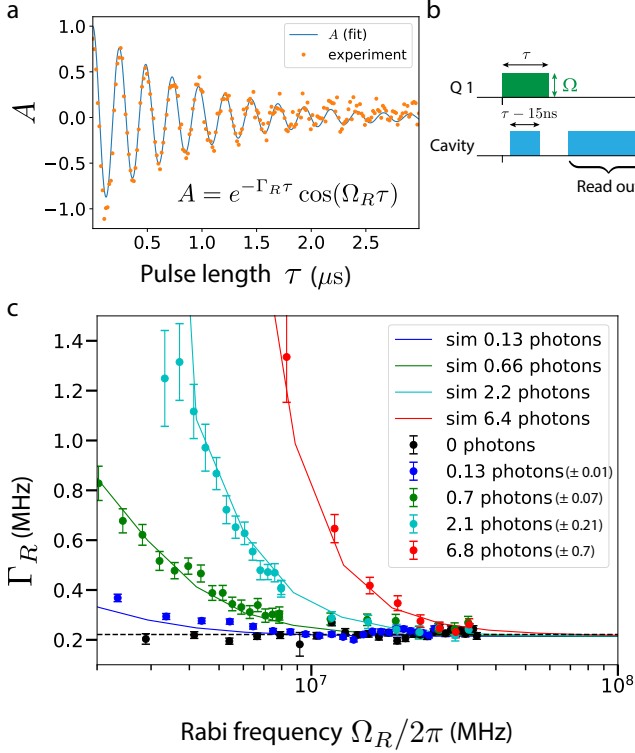


FIG. 3. **Rabi decay rates vs. Rabi frequency Ω_R for different measurement strengths.** **a**, Example of a rifled Rabi measurement ($\Omega_R/2\pi = 4.1$ MHz, $\langle n_{\text{photon}} \rangle \approx 2.1$) with overlaying numerical fit of the equation shown in the insert. **b**, Pulse protocol of the rifled Rabi measurement. The cavity pulse starts 10 ns after the qubit drive and stops 15 ns before its end. The actual read out pulse starts 5 ns after the qubit drive ends. **c**, Measured and simulated rifled Rabi and standard Rabi decay rates. For a fixed probe power, the Rabi decay rate is measured for increasing Rabi drives following the protocol presented in (b). The values for $\langle n_{\text{photon}} \rangle$ are measured independently via the ac-Stark shift. For the simulations, the average number of photons is extracted by normalizing to the fitted curve for the lowest measurement strength, which is assumed to match the measurement.

tions for Qubit 1 in the time domain and plot their decay rate in Figure 3c. Note that only a single fit parameter was used to scale the curve with lowest drive strength.

As it suppresses the measurement back-action, rifling allows measurements on other qubits coupled to the same detector, while keeping the rifled qubit in superposition.

To demonstrate this multiplexing capability, we perform a two-qubit algorithm with both qubits coupled to the same readout resonator (see Figure 4). First we prepare a superposition of the four basis states by applying a $R_y^{\pi/2}$ rotation to both qubits. We then rifle Qubit 1 for 1142 ns, while performing tomography on Qubit 2, followed by tomography on Qubit 1. We measure the density matrix of Qubit 1 with 92.8% fidelity (corrected for qubit decoherence), confirming the qubit remained

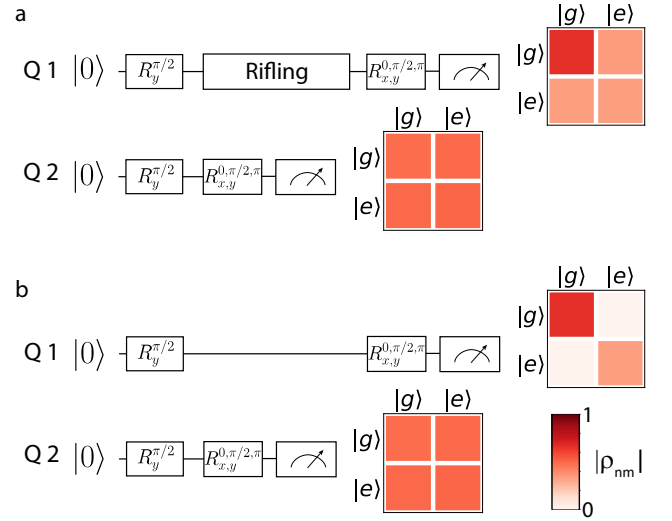


FIG. 4. **Sequential measurement of two qubits coupled to the same resonator with and without rifling.** **a**, Gate protocol and measured single qubit density matrices. First, both qubits are brought to full superposition by applying a $R_y^{\pi/2}$ rotation. Then Qubit 1 is rifled by applying a strong coherent Rabi drive for 1142 ns, while Qubit 2 is read out via tomography pulses followed by a cavity read out pulse, which ends before the Rabi drive pulse on Qubit 1. Lastly, Qubit 2 is read out. **b**, Same as in (a), but Qubit 1 is left idle for 1142 ns instead of rifling.

in superposition following the first read out (Figure 4a). Conversely, omitting the rifling pulse (Figure 4b) leads to vanishing non-diagonal terms in the density matrix and therefore to the collapse of coherence of Qubit 1, induced by the read out of Qubit 2.

It is worth noting that following the initial $R_y^{\pi/2}$ pulse, the qubit can be rotated around two different axes of the Bloch sphere: either around the x-axis, inducing full rotations around the Bloch sphere, or around the y-axis, effectively spin-locking the qubit[28]. We report that in both cases the coherence is preserved (see Supplementary information Sec. V.). We also performed rifling of Qubit 2 while extracting information from Qubit 1 with similar results (see Supplementary information Sec. VI.).

Other protocols to suppress measurement back-action on qubits[29–31] have been recently realized; contrary to quantum rifling, however, these methods require additional time-dependent pump drives beyond the Rabi drive and thus offer a less practical implementation. Interestingly, the merging of the two cavity peaks with increasing qubit modulation is reminiscent of motional averaging of a linewidth of a molecule[32]. In analogy, one could view our experiment as motional narrowing of the resonator, where the qubit acts as noisy environment shifting the resonator’s resonance frequency. Likewise, the absence of measurement dephasing for a fast rotating qubit bears similarities with dynamical decoupling schemes[33], where

noise during successive periods of free evolution interferes destructively at specific moments in time. In contrast, quantum riffling allows controlled decoupling of individual qubits from their measurement apparatus for all times during riffling. In addition, quantum riffling could be used to render eigenstates of a system indistinguishable and thus avoid the collapse of superposition if one wishes only to distinguish between larger submanifolds of the system. For example, if one tries to measure whether a qutrit is in its ground state or not without destroying the coherence between its first and second excited states, one can achieve this by driving the transition between the two excited states during measurement.

In conclusion, our results reveal an intuitive picture for the regime of a strongly driven, continuously measured qubit, where the Rabi frequency exceeds both the measurement rate and the meter bandwidth. In this regime, the resonator photons are not able to extract information about the qubit's state, leading to a time-averaged population measurement of the qubit and importantly imposing no back-action. We have also demonstrated that a strong Rabi drive can be utilized as an experimental knob to tune the measurement back-action between qubit and probe, without affecting the ability to measure other qubits probed simultaneously by the same field. This capability allows for many qubits to be connected to an individual detector, thus facilitating scalability in architectures where connecting individual detectors to every qubit might be technically challenging[34].

We thank Benjamin Huard, Gerard Milburn, Tom Stace and Sergey N. Shevchenko for fruitful discussions. This research was supported by the Australian Research Council Centre of Excellence for Engineered Quantum Systems (EQUS, CE170100009), the ARC Future Fellowship FT140100338 and by the Swiss National Science Foundation through the NCCR QSIT.

* Current address:daniel.szombati@ens-lyon.fr

- [1] W. Gerlach and O. Stern, *Zeitschrift für Physik* **9**, 349 (1922).
- [2] G. J. Milburn, *Journal of the Optical Society of America B* **5**, 1317 (1988).
- [3] A. Blais, R.-S. Huang, A. Wallraff, S. M. Girvin, and R. J. Schoelkopf, *Physical Review A* **69**, 62320 (2004).
- [4] J. Gambetta, A. Blais, M. Boissonneault, A. A. Houck, D. I. Schuster, and S. M. Girvin, *Phys. Rev. A* **77**, 012112 (2008).
- [5] M. Hatridge, S. Shankar, M. Mirrahimi, F. Schackert, K. Geerlings, T. Brecht, K. M. Sliwa, B. Abdo, L. Frunzio, S. M. Girvin, R. J. Schoelkopf, and M. H. Devoret, *Science* **339**, 178 (2013).
- [6] Q. Ficheux, S. Jezouin, Z. Leghtas, and B. Huard, *Nature Communications* **9**, 1926 (2018).
- [7] W. M. Itano, D. J. Heinzen, J. J. Bollinger, and D. J. Wineland, *Phys. Rev. A* **41**, 2295 (1990).
- [8] L. S. Schulman, *Phys. Rev. A* **57**, 1509 (1998).
- [9] E. W. Streed, J. Mun, M. Boyd, G. K. Campbell, P. Medley, W. Ketterle, and D. E. Pritchard, *Phys. Rev. Lett.* **97**, 260402 (2006).
- [10] R. Vijay, D. H. Slichter, and I. Siddiqi, *Phys. Rev. Lett.* **106**, 110502 (2011).
- [11] D. H. Slichter, C. Müller, R. Vijay, S. J. Weber, A. Blais, and I. Siddiqi, *New Journal of Physics* **18**, 053031 (2016).
- [12] Z. Mineev, S. Mundhada, S. Shankar, P. Reinhold, R. Gutiérrez-Jáuregui, R. Schoelkopf, M. Mirrahimi, H. Carmichael, and M. Devoret, *Nature* **570**, 200 (2019).
- [13] T. M. Stace and S. D. Barrett, *Phys. Rev. Lett.* **92**, 136802 (2004).
- [14] H.-S. Goan and G. J. Milburn, *Phys. Rev. B* **64**, 235307 (2001).
- [15] A. N. Korotkov and D. V. Averin, *Phys. Rev. B* **64**, 165310 (2001).
- [16] A. N. Korotkov, *Phys. Rev. B* **63**, 085312 (2001).
- [17] S. A. Gurvitz, L. Fedichkin, D. Mozyrsky, and G. P. Berman, *Phys. Rev. Lett.* **91**, 066801 (2003).
- [18] A. N. Jordan and M. Büttiker, *Phys. Rev. Lett.* **95**, 220401 (2005).
- [19] A. N. Jordan and A. N. Korotkov, *Phys. Rev. B* **74**, 085307 (2006).
- [20] A. N. Jordan, A. N. Korotkov, and M. Büttiker, *Phys. Rev. Lett.* **97**, 026805 (2006).
- [21] A. Palacios-Laloy, F. Mallet, F. Nguyen, P. Bertet, D. Vion, D. Esteve, and A. N. Korotkov, *Nature Physics* **6**, 442 (2010).
- [22] M. M. Maricq, *Phys. Rev. B* **25**, 6622 (1982).
- [23] J. Koch, T. M. Yu, J. Gambetta, A. A. Houck, D. I. Schuster, J. Majer, A. Blais, M. H. Devoret, S. M. Girvin, and R. J. Schoelkopf, *Phys. Rev. A* **76**, 042319 (2007).
- [24] G. Ithier, E. Collin, P. Joyez, P. J. Meeson, D. Vion, D. Esteve, F. Chiarello, A. Shnirman, Y. Makhlin, J. Schrieffer, and G. Schon, *Phys. Rev. B* **72**, 1 (2005).
- [25] J. R. Johansson, P. D. Nation, and F. Nori, *Computer Physics Communications* **184**, 1234 (2013).
- [26] D. A. Golter, T. K. Baldwin, and H. Wang, *Phys. Rev. Lett.* **113**, 237601 (2014).
- [27] A. Laucht, R. Kalra, S. Simmons, J. P. Dehollain, J. T. Muhonen, F. A. Mohiyaddin, S. Freer, F. E. Hudson, K. M. Itoh, D. N. Jamieson, J. C. McCallum, A. S. Dzurak, and A. Morello, *Nature Nanotechnology* **12**, 61 (2016).
- [28] F. Yan, S. Gustavsson, J. Bylander, X. Jin, F. Yoshihara, D. G. Cory, Y. Nakamura, T. P. Orlando, and W. D. Oliver, *Nature Communications* **4**, 2337 (2013).
- [29] J. Suh, A. J. Weinstein, C. U. Lei, E. E. Wollman, S. K. Steinke, P. Meystre, A. A. Clerk, and K. C. Schwab, *Science* **344**, 1262 (2014).
- [30] S. Touzard, A. Kou, N. E. Frattini, V. V. Sivak, S. Puri, A. Grimm, L. Frunzio, S. Shankar, and M. H. Devoret, *Phys. Rev. Lett.* **122**, 080502 (2019).
- [31] T. Peronin, D. Marković, Q. Ficheux, and B. Huard, arXiv preprint arXiv:1904.04635 (2019).
- [32] J. Li, M. P. Silveri, K. S. Kumar, J.-M. Pirkkalainen, A. Vepsäläinen, W. C. Chien, J. Tuorila, M. A. Sillanpää, P. J. Hakonen, E. V. Thuneberg, and G. S. Paraoanu, *Nature Communications* **4**, 1420 (2013).
- [33] J. Bylander, S. Gustavsson, F. Yan, F. Yoshihara, K. Harrabi, G. Fitch, D. G. Cory, Y. Nakamura, J. S. Tsai, and W. D. Oliver, *Nature Physics* **7**, 565 (2011).
- [34] J. Heinsoo, C. K. Andersen, A. Remm, S. Krinner, T. Walter, Y. Salathé, S. Gasparinetti, J.-C. Besse, A. Potočnik,

A. Wallraff, and C. Eichler, *Phys. Rev. Applied* **10**, 034040 (2018).